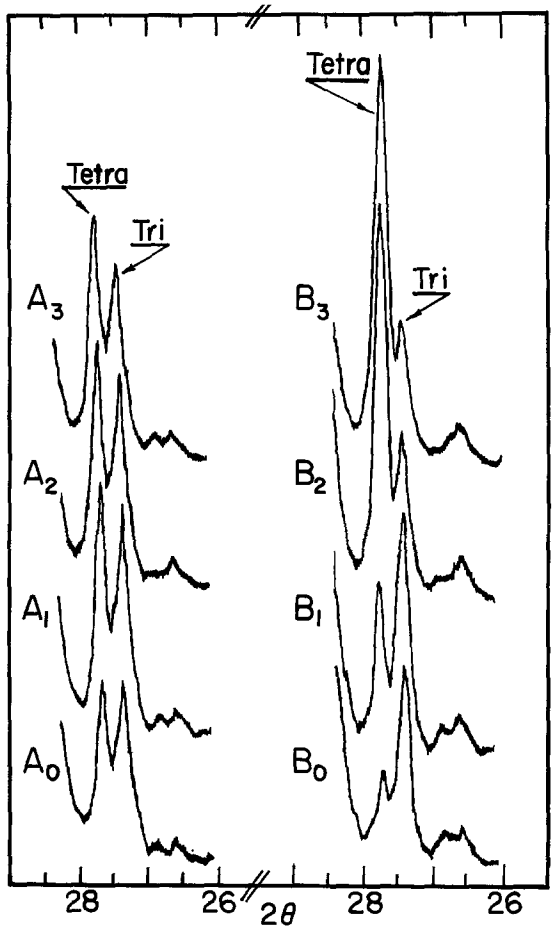

Fig. 8. X-ray diffraction patterns of two examples (A_0 and B_0) of pastes prepared from Anachemia PbO (No. 2a) and $PbSO_4$, and cured at room temperature for 4 weeks. They were then ground and suspended in water at room temperature for 1 day (A_1 and B_1), 4 days (A_2 and B_2), and 10 days (A_3 and B_3).

5 and 8. The nucleation process is evidently much slower for the reaction with crystalline $3PbO \cdot PbSO_4 \cdot H_2O$. This suggests that the nucleation site is the ternary interface between the aqueous phase, a growing structure energetically close to tribasic sulfate and the PbO surface, one that, in a quiescent state, would be well established and have a high *p*H. With tribasic sulfate as the added reactant, and in a well-crystallized form, such an interface may not readily be formed.

All the evidence seems to suggest that, in the presence of excess PbO, $4PbO \cdot PbSO_4$ is the stable sulfate at room temperature. If so, further studies on the $PbO-SO_3-H_2O$ system, its thermodynamic aspects and potential-*p*H diagram, are warranted.

Acknowledgment

This work was supported, in part, by the Industrial Research Assistance Program of the National Research Council of Canada. Most of the experimental work was done by N. A. Haneke and R. J. Lloyd.

Manuscript received Aug. 12, 1980. This was Paper 13 presented at the Las Vegas, Nevada, Meeting of the Society, Oct. 17-22, 1976.

Any discussion of this paper will appear in a Discussion Section to be published in the December 1981 JOURNAL. All discussions for the December 1981 Discussion Section should be submitted by Aug. 1, 1981.

Publication costs of this article were assisted by Cominco Limited.

REFERENCES

1. J. Burbank, *This Journal*, **113**, 10 (1966).
2. R. V. Biagetti and M. C. Weeks, *Bell Syst. Tech. J.*, **49**, 1305 (1970).
3. C. F. Yarnell, U.S. Pat. 3,788,898 (1974).
4. R. V. Biagetti, U.S. Pat. 3,765,943 (1973).
5. C. F. Yarnell, *This Journal*, **125**, 1934 (1978).
6. C. F. Yarnell and M. C. Weeks, *ibid.*, **126**, 8 (1979).
7. H. Bode and E. Voss, *Electrochim. Acta*, **1**, 318 (1959).
8. S. Ikari, S. Yoshizawa, and S. Okada, *J. Electrochem. Soc. Jpn.*, **27**, E-167 (1959).
9. S. C. Barnes and R. T. Mathieson, in "Batteries 2," D. H. Collins, Editor, p. 41, Pergamon Press, Oxford (1965).
10. A. C. Simon and E. L. Jones, *This Journal*, **109**, 760 (1962).
11. K. R. Bullock, *ibid.*, **127**, 662 (1980).
12. D. Pavlov and G. Papazov, *J. Appl. Electrochem.*, **6**, 339 (1976).
13. V. Iliev and D. Pavlov, *ibid.*, **9**, 555 (1979).
14. J. N. Mrgudich, *Trans. Electrochem. Soc.*, **81**, 165 (1942).
15. M. Denby, in "Batteries," D. H. Collins, Editor, p. 439, The MacMillan Company, New York (1963).
16. N. E. Hehner and E. J. Ritchie, "Lead Oxides, Chemistry–Technology–Battery Manufacturing Uses—History," Independent Battery Manufacturers Assoc., Inc., (1974).

All-Solid Lithium Electrodes with Mixed-Conductor Matrix

B. A. Boukamp,* G. C. Lesh, and R. A. Huggins*

Department of Materials Science and Engineering, Stanford University, Stanford California 94305

ABSTRACT

The concept of a novel all-solid composite electrode is presented. One example of such a composite contains a finely dispersed reactant, Li_ySi, in a solid mixed-conducting matrix, $Li_{2.6}Sn$. Repeated charging and discharging of such electrodes without appreciable loss of capacity has been demonstrated. The polarization is found to be comparable to values typical of highly porous electrode systems in molten salt electrolytes.

The use of elemental lithium electrodes in high temperature lithium/metal sulfide battery systems presents serious problems, as it is highly corrosive, difficult to contain, and dissolves in the molten salt electrolyte causing severe self-discharge. These problems can be reduced by using solid lithium-metal alloys which have a lower lithium activity. In order to provide high current densities, these electrodes are typically made as a highly porous salt-filled sponge [Li-Al

* Electrochemical Society Active Member.
Key words: composite, battery electrodes, chemical diffusion, lithium-silicon, lithium-tin.

system (1, 2)], or as a powder contained in a mesh cage [Li-Si system (3, 4)]. Such lithium-metal alloys are often found to lose capacity with cycling.

A different approach, an all-solid composite electrode, which has the potential of being an attractive alternative is presented here. This composite has a microstructure in which a reactant, (*e.g.*, Li_yAl or Li_ySi) is finely dispersed in a solid mixed-conducting matrix, so that there is a large (internal) reactant surface area. The compound that is used as the matrix phase should be a good electronic conductor, should have a high diffusion constant for the electroactive species (*e.g.*, Li), and except for the transfer of the electroactive species, should not react with the reactant phase. It must also be stable over the range of potential at which the reactant is operated. The matrix phase determines and maintains the microstructural morphology of the dispersed reactant, is the current collector, and is also a fast transport medium for the electroactive species, while the reactant acts as the storage system.

While some preliminary experiments have been performed with different combinations of reactants and matrix compositions, the data presented here, showing the feasibility of this concept, deal with experiments done on the $Li_ySi/Li_{2.6}Sn$ system. The important electrochemical and structural parameters are given in the next two paragraphs.

A number of phases exist in the Li-Sn system (5-11). They all exhibit rather high chemical diffusion for Li (12). The $Li_{2.6}Sn$ (or $Li_{13}Sn_5$) phase has the highest chemical diffusion constant, with $\tilde{D}_{Li} = 5 \times 10^{-5}$ increasing to 7.6×10^{-4} cm²/sec with increasing lithium activity at 415°C, which is even greater than typical molten salt values of $1\text{-}5 \times 10^{-5}$ cm²/sec. The stability range of this phase is between 0.390 and 0.286V with respect to lithium at 415°C (5) (for increasing a_{Li}). The position of all Li-Sn phases and two-phase voltage plateaus is given in Fig. 1, together with those for the reactant, Li_ySi. The variation in stoichiometry, δ, for $Li_{13+\delta}Sn_5$, is small, ranging from -0.04 to $+0.025$ with increasing a_{Li} (12). The volume per Sn atom varies with increasing Li content, in some cases causing appreciable volume changes upon the conversion of one Li-Sn phase into the next. The important parameters pertaining to this are given in Table I.

Much doubt has existed about the true compositions of the Li-Si phases. Recent electrochemical measurements in our laboratory (13, 14) and careful x-ray analysis elsewhere (11, 15-18) have shown that the phases in the Li-Si system are $Li_{1.71}Si$ (or $Li_{12}Si_7$) (15), $Li_{2.33}Si$ (or $Li_{14}Si_6$) (16), $Li_{3.25}Si$ (or $Li_{13}Si_4$) (17), and $Li_{4.4}Si$, (or $Li_{22}Si_5$). The stability ranges of these phases with respect to the lithium activity, and the two-phase voltage plateaus according to Ref. (13) and (19-21) are given in Fig. 1. From this figure it is clearly seen that the Si-$Li_{1.71}Si$ two-phase plateau voltage is positioned in the middle of the stability range of the matrix phase $Li_{2.6}Sn$.

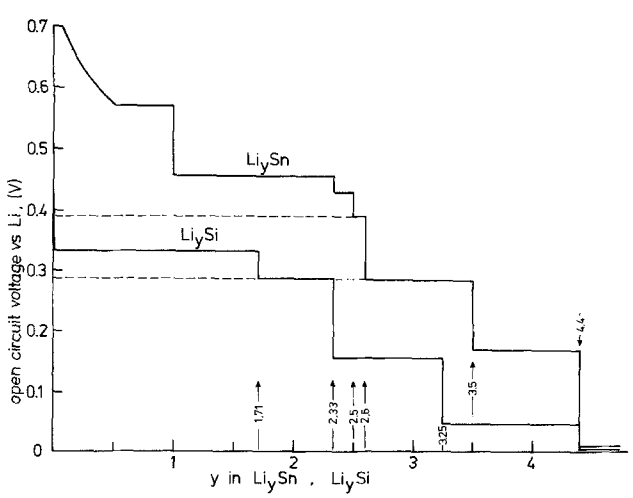

Fig. 1. Coulometric titration curve showing two-phase plateaus and ranges of stability of single phases for the Li-Sn (5) and Li-Si (13, 19-21) systems.

Table I. Crystal structure, unit cell volume, number of formula units per unit cell, crystal volume per Sn atom, and theoretical density for the Li-Sn system

Compound and crystal structure	Unit cell volume (Å³)	Formula units per unit cell	Volume per Sn-atom (Å³)	Theoretical density (g/cm³)	Ref.
LiSn					
Monoclinic	132.2	3	41.1	5.07	(6, 7)
Li_7Sn_3, ($Li_{2.33}Sn$)					
Monoclinic	367.1	2	61.2	3.66	(8)
Li_5Sn_2, ($Li_{2.5}Sn$)					
Rhombohedral	385.8	3	64.3	3.51	(9)
$Li_{13}Sn_5$, ($Li_{2.6}Sn$)					
Hexagonal	327.5	1	65.5	3.47	(10)
Li_7Sn_2, ($Li_{3.5}Sn$)					
Orthorhombic	642.4	4	80.3	2.96	(7)
$Li_{22}Sn_5$, ($Li_{4.4}Sn$)					
Cubic	773.9	16	96.7	2.56	(11)

Experimental Procedures

The matrix, Li_ySn, was prepared by the careful addition of lithium (99.9%, Alfa) to molten tin (99.9%, Baker) in a molybdenum crucible at ~ 400°C followed by heating to 600°C for 20-30 min. The crucible was closed, but not tightly sealed, with a molybdenum lid. After rapid cooling by removal of the crucible from the furnace, the metallic gray product was broken in a mortar and milled to a fine powder in a ball mill. All handling was done in a helium atmosphere glove box, or in a protective, leak-tight enclosure. No chemical analysis was necessary, as the composition could be readily determined by electrochemical titration.

The matrix material was then mixed and ground with Si powder (99.95%, Alfa) in a mortar, the Si/Sn ratio being 0.617. The particle size of 90% of the powder mixture was smaller than 45 micron. Pellets were pressed from this mixture in either 3/8 in. (0.93 cm) or 5/16 in. (0.794 cm) diameter evacuated steel dies at a pressure of 2700 kg/cm². This resulted in an overall density over 80% of the theoretical value. This is considerably greater than that typically found in finely divided porous electrodes. The pellets were then placed in a molybdenum holder which was tightened around the cylindrical edge of the sample, exposing the flat planparallel surfaces to the molten electrolyte.

Reference and counterelectrodes were prepared in the same manner using an Al/LiAl mixture of nominal

Table II. Crystal structure, unit cell volume, formula units per unit cell, crystal volume per Si atom, and theoretical density for the Li-Si system

Compound and crystal structure	Unit cell volume (Å³)	Formula units per unit cell	Volume per Si-atom (Å³)	Theoretical density (g/cm³)	Ref.
Si					
Cubic	160.2	8	20.0	2.33	
$Li_{12}Si_7$, ($Li_{1.71}Si$)					
Orthorhombic	2436	6	58.0	1.15	(15)
$Li_{14}Si_6$, ($Li_{2.33}Si$)					
Rhombohedral	308.9	1	51.5	1.43	(16)
$Li_{13}Si_4$, ($Li_{3.25}Si$)					
Orthorhombic	538.4	2	67.3	1.38	(17)
$Li_{22}Si_5$, ($Li_{4.4}Si$)					
Cubic	6592	16	82.4	1.18	(11, 18)

overall composition $Li_{0.82}Al$. The three electrode system (LiAl/Al counter and reference; Li-Sn-Si working electrode) was then placed in the molten LiCl-KCl electrolyte (Lithcoa), contained in an Al_2O_3 crucible in a furnace, the temperature being maintained at ~ 410°C. The electrochemical experiments also were carried out in a helium atmosphere glove box.

Experiments were performed using an Aardvark Model V potentiostat/galvanostat, an Aardvark Model BA-1 buffer amplifier, and a Model 379 PAR digital coulometer. Voltages were measured using a Keithley digital multimeter and a stripchart recorder. Experiments were either performed potentiostatically or galvanostatically.

Experiments and Results

Experiments were performed on electrode systems in which the starting composition of the matrix was $Li_{1.56}Sn$, (or LiSn + 0.74 $Li_{2.33}Sn$). Lithium was added electrochemically to the sample until its potential reached 0.350V with respect to lithium. At this point virtually no lithium has been incorporated in the single-phase Si reactant, as the solubility of Li in silicon has been estimated to be less than 0.36 atomic percent (a/o) at 415°C (13). The matrix then goes through two phases, $Li_{2.33}Sn$ and $Li_{2.5}Sn$, before arriving at the equilibrium composition $Li_{2.6}Sn$. The influence of this recrystallization process upon the mechanical strength of the sample is still under investigation.

The first few charging (adding lithium to the reactant) and discharging (removing lithium from the reactant) cycles were performed potentiostatically, the charging potential being set at 0.300V *vs.* Li and the discharging potential at 0.375 *vs.* Li. The current was integrated by a coulometer and recorded on a stripchart recorder. In this way the capacity of the reactant could be measured. The coulombic capacity was found to be within the experimental error of the calculated value for the Si-$Li_{1.71}Si$ plateau. During the course of the experiment potentiostatic cycles were run in order to monitor the coulombic capacity. It was found that it remained virtually constant over the duration of the experiments (16-20 cycles, one charge and discharge counted as one cycle) indicating negligible capacity loss on cycling.

During this potentiostatic cycling possible slow second phase nucleation was observed for the reactant. At the onset of the charge or discharge cycle the current had an initial high value, which decreased rapidly due to the small change in stoichiometry of the matrix phase which is associated with the instantaneous change in lithium activity. The current then went through a minimum which is probably associated with the slow nucleation of the second phase ($Li_{1.71}Si$ for the charge and Li-saturated Si for the discharge cycle) as under this potentiostatic cycling the reactant is driven into its single-phase regime.

A number of cycles were performed galvanostatically in order to establish the polarization characteristics of the mixed-conducting matrix electrodes. No special precaution was taken with respect to the placement of the electrodes; a simple triangular arrangement was used. In order to start from the same composition, or lithium activity, the electrodes were equilibrated potentiostatically at 0.375V *vs.* Li before charge, and 0.300V before discharge. Thus, as each cycle started with a single-phase reactant, what appeared to be slow second-phase nucleation again was observed as a voltage dip in the polarization at the onset of the charge cycle, and a voltage peak at the onset of the discharge cycle, as shown in Fig. 2.

When the galvanostatic charge and discharge cycles were terminated before reaching the ends of the two-phase plateau, this slow second-phase nucleation was not observed, as both phases were then always present in the reactant (see Fig. 3).

The overpotential as a function of the current density (taking both sides of the sample into account) is

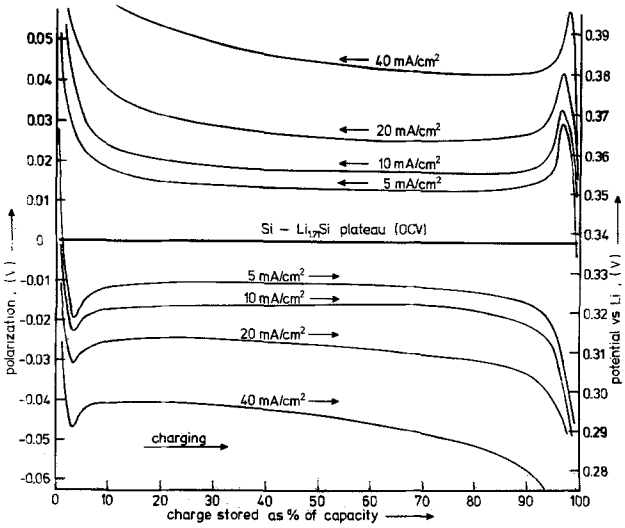

Fig. 2. Electrode polarization as function of the state of charge for several current densities.

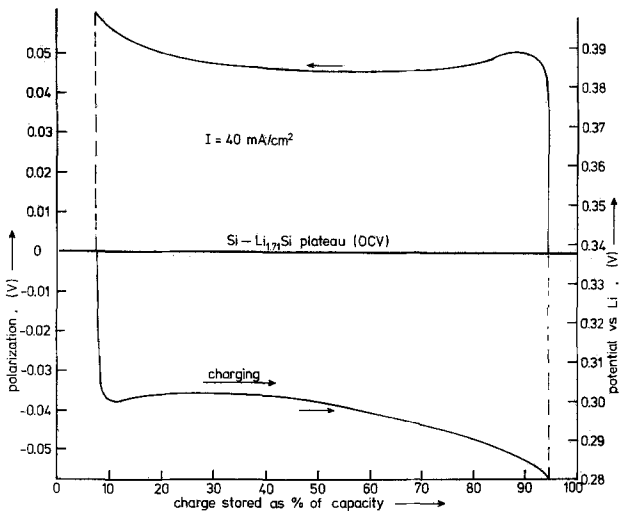

Fig. 3. Electrode polarization as function of the state of charge demonstrating the disappearance of the nucleation related dips and peaks when not cycled to the ends of the plateau.

shown for a 50% state of charge in Fig. 4. The overpotential was found to be small, of the order of 1 mV per mA per cm² of macroscopic surface area, being slightly larger near the end of the charge or discharge cycle.

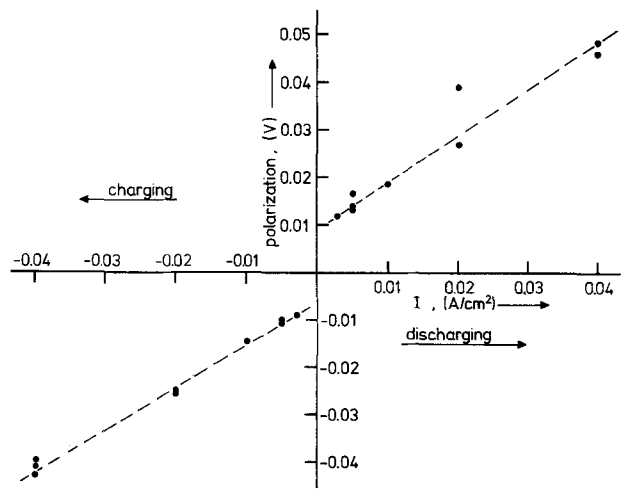

Fig. 4. Electrode polarization as function of the current density for a state of 50% charge stored.

If the matrix electrode is charged with more lithium the potential falls to that of the next two-phase plateau where $Li_{2.33}Si$ begins to form. The matrix could also enter a two-phase region with the formation of $Li_{3.5}Sn$ at about the same potential [0.282V *vs.* Li for $Li_{1.71}Si/Li_{2.33}Si$ (19-21) and 0.286V *vs.* Li for $Li_{2.6}Sn/Li_{3.5}Sn$ (5)].

Figure 5 shows a complete galvanostatic cycle, measured at a current density of 5 mA/cm^2 in which the two additional plateaus can be observed. From the length of these plateaus it follows that the first additional plateau is the $Li_{1.71}Si/Li_{2.33}Si$ two-phase region, as its length is $\sim$ 0.3 times the length of the first, *i.e.*, Si-$Li_{1.71}Si$, plateau. The OCV was measured to be 0.288V at 410°C, the same as found by Ref. (13), but slightly higher than reported by Ref. (19-21). The second additional plateau is associated with the $Li_{2.6}Sn/Li_{3.5}Sn$ two-phase region. Its length was equivalent to about 0.9 times the amount of Sn in the sample. The OCV for this plateau was measured to be 0.276V *vs.* Li, (at 410°C) which is 10 mV lower than reported by (5).

These extended charging and subsequent discharging did not seem to affect the integrity of the sample, or the overall kinetic behavior of the electrode. The coulombic capacity of the first plateau remained virtually unchanged.

Discussion

In the preceding section the feasibility of this mixed conducting matrix electrode concept has been clearly demonstrated. It is, however, important to discuss its merits with regard to the conventional porous, salt-filled electrodes. The solid matrix phase is obviously heavier than the chloride molten salt which typically exists in the pores of electrode structures prepared by the consolidation, or mechanical containment, of powders (the density of $Li_{2.6}Sn$ is 3.47 g/cm^3, whereas the density of the eutectic composition of the LiCl-KCl salt is 1.66 g/cm^3). The matrix phase acts, on the other hand, simultaneously as the current collector, so no additional material needs to be included for that purpose. Nor is a metallic (*e.g.*, nickel, which has a density of 8.90 g/cm^3) sponge necessary to hold the reactant powder in place.

While this may lead to a slight loss of weight efficiency in this approach, there could be kinetic advantages, as the chemical diffusion coefficient is greater in this metallic matrix than the typical value of about 10^{-5} cm^2/sec for molten salts. In this way the possibility of electrolyte freezing inside the pores of the salt-filled electrodes, due to a local depletion or enrichment of Li in the eutectic electrolyte (22) is avoided.

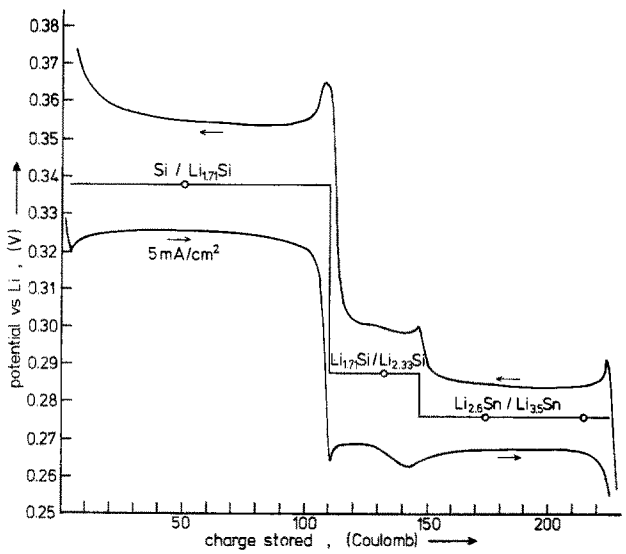

Fig. 5. Electrode polarization at 5 mA/cm^2 as function of the charge stored during a complete charge-discharge cycle to lower voltages. The circles represent measured open-circuit voltages.

The theoretical coulombic capacity of such an electrode with an Si/Sn atom ratio of 0.62, operated only within the first Li-Si two-phase region is 0.46 A-hr/cm^3. In comparison, the "contained powder" Li-Si electrode of Seefurth and Sharma (3, 4) contained 0.68 A-hr/cm^3 when charged to the same Li/Si atom ratio. If the composite electrode were utilized to higher Li contents, *i.e.*, to $Li_{3.5}Sn$ and $Li_{2.33}Si$, which involved reaction with both the silicon and the tin, the capacity increases to 0.93 A-hr/cm^3. Under these conditions, the pure Li-Si electrode of Seefurth and Sharma also has 0.93 A-hr/cm^3. The measured overvoltages were somewhat larger than those measured by Seefurth and Sharma (3, 4) although no corrections for electrolyte resistance were applied.

Although there have not been very many experiments to data, present indications are that there is negligible loss of capacity upon cycling electrodes with this type of composite structure. This is what would be expected if the microstructure returned to its original state after the completion of each full cycle.

This approach avoids the typical problems of densification and particle growth which often play a role in decreasing the useful capacity in conventional liquid-permeated electrode structures.

Further work is being undertaken to investigate the microstructural features of the operation of such composite electrodes as well as their range of applicability.

Acknowledgment

This work was supported by the U.S. Department of Energy under LBL Subcontract No. 4503110.

Manuscript submitted July 1, 1980; revised manuscript received Nov. 10, 1980.

Any discussion of this paper will appear in a Discussion Section to be published in the December 1981 JOURNAL. All discussions for the December 1981 Discussion Section should be submitted by Aug. 1, 1981.

Publication costs of this article were assisted by Stanford University.

REFERENCES

1. N. P. Yao, L. A. Heredy, and R. C. Saunders, *This Journal*, **118**, 1039 (1971).
2. E. C. Gay, D. R. Vissers, F. J. Martino, and K. E. Anderson, *ibid.*, **123**, 1591 (1976).
3. R. N. Seefurth and R. A. Sharma, *ibid.*, **124**, 1207 (1977).
4. R. N. Seefurth and R. A. Sharma, *ibid.*, **127**, 1101 (1980).
5. C. J. Wen and R. A. Huggins, *ibid.*, To be published.
6. W. Muller and H. Schafer, *Z. Naturforsch.*, **28b**, 246 (1973).
7. U. Frank, W. Muller, and H. Schafer, *ibid.*, **30b**, 6 (1975).
8. W. Muller, *ibid.*, **29b**, 304 (1974).
9. U. Frank, W. Muller, and H. Schafer, *ibid.*, **30b**, 1 (1975).
10. U. Frank and W. Muller, *ibid.*, **30b**, 316 (1975).
11. E. I. Gladyshevskii, G. I. Oleksov, and P. I. Kripyakevich, *Sov. Phys.-Cryst.*, **9**, 269 (1964).
12. C. J. Wen and R. A. Huggins, *J. Solid State Chem.*, To be published.
13. C. J. Wen, Ph.D. Dissertation, Stanford University (1980).
14. C. J. Wen and R. A. Huggins, *J. Solid State Chem.*, To be published.
15. H. G. von Schnering, R. Nesper, K.-F. Tebbe, and J. Curda, Unpublished results (1980).
16. H. G. von Schnering, R. Nesper, K.-F. Tebbe, and J. Curda, *Z. Metallk.*, **71**, 357 (1980).
17. U. Frank, W. Muller, and H. Schafer, *Z. Naturforsch.*, **30b**, 10 (1975).
18. H. Axel, H. Schafer, and A. Weiss, *ibid.*, **21b**, 115 (1966).
19. R. A. Sharma and R. N. Seefurth, *This Journal*, **123**,

1763 (1976).
20. L. R. McCoy and S.-C. Lai, in "Proceedings of the Symposium and Workshop on Advanced Battery Research and Design," U.S. ERDA Report No. ANL-76-8, p. B-167, March, 1976.
21. S.-C. Lai, *This Journal*, **123**, 1196 (1976).
22. J. Braunstein and C. E. Vallet, *ibid.*, **126**, 960 (1979).

Influence of the Growth Conditions of Al_2O_3 Passivating Layers on the Corrosion of Aluminum Films in Water

J. Grimblot[1] and J. M. Eldridge

IBM Research Laboratory, San Jose, California 95193

ABSTRACT

The effects of water vapor on the oxidation kinetics of UHV-deposited Al films have been investigated using *in situ* ellipsometric measurements. For a given exposure time, the presence of ~33% H_2O increases the Al_2O_3 thickness by ~50% and roughly doubles the extinction coefficient of the oxide. We attribute the nonzero extinction coefficients (with a range in values from 0.05 to 0.18) as being due to the presence of excess Al in the oxide. The "wet"-grown Al_2O_3 layers oxidize at least twice as fast as "dry"-grown layers on storing of samples in a normal laboratory environment. Furthermore, the relative effectiveness of the passivation provided to the underlying Al is greater for the "dry"- than the "wet"-grown Al_2O_3 layers. Gravimetric and electrical resistance data from samples exposed to an aqueous corrosion test are given to support this.

The lifetimes of Al conductor lines in integrated circuits is highly dependent on the quality of the thin (~20Å) air-formed Al_2O_3 layer. In an effort to better understand processing effects on Al_2O_3 quality as a passivant, *in situ* ellipsometry studies have been used to evaluate the growth and optical properties of oxide layers grown in dry O_2 on UHV-deposited Al films (1). The sensitivity afforded by this approach has clearly shown that the reaction rate is not significantly pressure sensitive and only moderately temperature dependent.

In this paper we report on the effects of water vapor on the oxide growth and properties, as determined by *in situ* ellipsometric measurements. Electrical resistance and weight change determinations were carried out *ex situ* to compare the passivating characteristics of "dry" and "wet" grown Al_2O_3.

Al films (2000Å thick) were deposited under UHV conditions as described elsewhere (1), and exhibited a very strong (111) preferred orientation. The effects of moisture [up to 33 volume percent (v/o)] on Al oxidation at 274°C is shown in Fig. 1. The data are presented according to a direct logarithmic growth law, although our earlier analysis (1) suggests the well-known Mott-Cabrera inverse log law is probably more correct. Note that the presence of 33% water increases the oxide thickness by roughly 50%.

As reported for the Al-dry O_2 reaction (2), the oxide layer is slightly light-absorbing at $\lambda = 5461$Å. For dry O_2, the optical extinction coefficient (k) of thin Al_2O_3 layers varies from 0.07 to 0.05 as the oxide grows from roughly 20 to 30Å. For "wet" grown oxides, k varies from ~0.18 to 0.10 for the same thickness range. We attribute the small light absorption as being due to the presence of a very small (~10^{19}/cm^3) concentration of Al atoms in excess of the stoichiometric ratio. Similar effects have been seen in the In_2O_3-In system (2).

We have attempted to use *ex situ* ellipsometric measurements in an effort to compare the relative passivities provided by the "dry" and "wet" Al_2O_3 layers. However, the results were quite difficult to interpret, perhaps owing to the formation of quite discontinuous islands of hydroxide, pits, blisters, etc. Indeed, it may only be possible to study the very initial reaction of materials in corrosive solutions via ellipsometry (3). Accordingly, we used ellipsometry here to measure thickness increases of the above oxides due to prolonged exposure to laboratory air (*i.e.*, ~25°C, 40-50% RH, and some unknown levels of corrosive pollutants). For periods up to roughly 40 days, we found the "wet" Al_2O_3 layers continued to grow in ambient air at ~1 Å/day, whereas "dry" Al_2O_3 grew at ~0.4 Å/day.

In an effort to better differentiate between the reactivity of these oxides, more extensive tests were conducted using various aqueous reactive ambients. We regard the aqueous test results as significant because: DI-water rinses are integral to all IC processing (4);

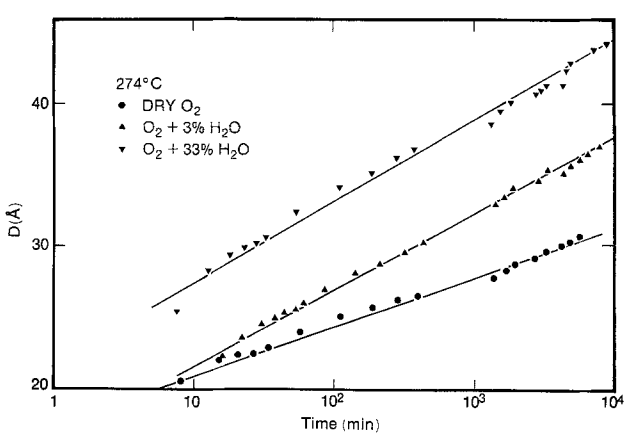

Fig. 1. Plot of the thickness as a function of log time (min). ● Dry O_2 (50 Torr) at 274°C; ▲ O_2 + 3% H_2O (50 Torr total pressure) at 274°C; ▼ O_2 + 33% H_2O (100 Torr total pressure) at 274°C.

[1] Permanent address: Université des Sciences et Techniques, Lille, France.

Key words: accelerated corrosion, thin films, semiconductor reliability.